

Research on a Rapid Method for Obtaining the Matching Point of the Static Operating Pressure of a Supersonic Jet in a Wind Tunnel

Peng Liu ✉ – Jinglun Cai – Xuejing Shao – Hui Jin
Qingdao University of Technology, School of Mechanical and Automotive Engineering, China
✉ peng_liu@qut.edu.cn

Abstract *In the wind tunnel test, mismatched operating pressures can cause the jet flow field to produce expansion waves, compression waves, and wave interference. The current wind tunnel pressure matching study requires continuous adjustment of the operating pressure at the inlet and outlet to obtain an ideal supersonic jet in an expanded state, and the pressure matching workload is substantial. This study presents a numerical simulation of the flow field of a supersonic wind tunnel under different outlet pressures based on the Reynolds-averaged Navier-Stokes (RANS) method. A method for quickly obtaining the static operating pressure matching point of a supersonic jet is proposed, which can quickly determine the matching operating pressure. When the Mach number of the monitoring point on the axis of the core area of the jet is within 5 % of the standard Mach number at the nozzle outlet, the jet in the wind tunnel test chamber is in an ideal expansion state, and the outlet pressure under this condition is the standard operating pressure for pressure matching. At the same time, the flow field structures under the conditions of over-expansion, ideal expansion, and under-expansion were compared, and it was shown that the key physical parameters in the core region of the supersonic jet field under the ideal expansion state obtained by this rapid matching method were stably distributed, which allowed the uniform region of the jet to exceed the limits of the diamond region and achieve uniform flow within the boundary of the supersonic jet.*

Keywords *supersonic jet, pressure matching, expansion wave, compression wave*

Highlights

- *A fast method for obtaining back pressure matching points in supersonic wind tunnels is presented.*
- *Analyzed jet field structure and flow distribution in the core under non-matching parameters.*
- *Described shear layer development, vortex shedding, and large-scale vortex interactions.*

1 INTRODUCTION

A full understanding of the flow field characteristics of supersonic vehicles is of great significance for the research and development and performance optimization of supersonic vehicles. The quality of the wind tunnel test will have a significant impact on the design and concept verification of the aircraft, aerodynamic optimization, stability and control, flight characteristics simulation, noise testing, structural load analysis, and verification of simulation results.

In the supersonic wind tunnel test, the airflow is ejected from the nozzle outlet and directly impacts the low-speed gas in the test chamber without the constraint of solid wall boundaries. This strong impact and the collision of the jet with the object to be tested in the chamber change the state of the jet, forming a complex unsteady flow field in the confined space of the test chamber. In the shear layer of the supersonic jet, the vortex structures generated by the vortex shedding will continue to develop and evolve. These vortex structures interact with the rear collection device, and the pressure will change accordingly, showing strong pressure pulsations and making the instability of the flow field more obvious. For example, Liu et al. [1] studied the changes in the structure and turbulence characteristics of the boundary layer caused by the injection of the inner wall surface and the auxiliary injection of the scramjet engine through an experimental-based research method supplemented by numerical simulation. Sun et al. [2] studied the turbulent characteristics of the disturbed concave curvature boundary layer near the wall surface in a wind tunnel through numerical simulation.

Sabnis et al. [3] studied the interaction of the shock boundary layer in a supersonic wind tunnel with a nozzle geometry, explaining the importance of considering a uniform flow field in wind tunnel tests of shock-boundary-layer interaction. Sandham and Reynolds [4] studied three-dimensional transonic mixing-layer flows using direct numerical simulation (DNS). Vreman et al. [5] studied the effect of compressibility on the growth rate of the mixing layer using DNS. Flow characteristics such as Mach number, total and static pressure, total temperature and static temperature, as well as turbulent viscosity ratio distribution and heat flux density at the wind tunnel wall were investigated with the aim of improving the quality of the flow and expanding the scope of wind tunnel tests by Drozdov and Rtishcheva [6].

Lu et al. [7] conducted an experimental study on the interaction between shock waves and turbulent boundary layers in the Mach 3.4 supersonic low-noise wind tunnel. Lu et al. [8] also conducted an experimental study of the transition process of the 5° smooth straight cone boundary layer in the Mach 6 supersonic low-noise wind tunnel, and analyzed the instantaneous fine structure of the conical boundary layer under different attack angles and different unit Reynolds numbers. Egorov et al. [9] analyzed the influence of the amplitude of the incident Mach wave on the transition from laminar to turbulent flow in the supersonic boundary layer based on numerical simulation.

In the study of the design and flow field analysis of the supersonic wind tunnel, Junmou et al. [10] designed an integrated supersonic nozzle with a Mach 1.5 and 2 by using the non-viscous contour characteristic curve and correcting the overall curve of the boundary layer, which made the uniform area of the wind tunnel jet break through the limitation of the diamond-shaped area. Gounko and Kavun [11] used the Reynolds-averaged Navier-Stokes (RANS) equations and the SST k–ω turbulence model to study the unsteady

 DOI: 10.5545/sv-jme.2024.1199

flow characteristics formed during the pulse start-up process of a supersonic wind tunnel with different diffusers. Kosinov et al. [12] experimentally studied the effect of a small angle of attack on the transition from laminar to turbulent flow in the supersonic boundary layer of a swept wing with a leading edge sweep angle of 72°.

Yu et al. [13] studied the starting characteristics of the wind tunnel in combination with the inlet model. The results show that a sudden increase in total pressure can generate a moving shock wave of sufficient strength to overcome the structure of the separation zone near the wind tunnel wall. Egorov et al. [14] used direct numerical simulation to simulate the roughness of the wind tunnel side wall in the boundary layer and then studied the effect of the incident Mach wave intensity on the laminar-turbulent transition (LTT). Bottini et al. [15] introduced the design of a Mach number supersonic wind tunnel for inducing boundary layer transition and analyzed the test intensity of free flow fluctuations. Wu et al. [16] performed RANS simulations on a supersonic wind tunnel with a perforated plate installed in a tandem nozzle, qualitatively analyzing the influence of the flow model on the synthetic flow field and the influence of the perforated plate on the flow quality in the test section.

Zhao et al. [17] analyzed the drag effect of hypersonic cones on free flow and found that hypersonic flow can reduce the skin friction between the main flow and the hypersonic jet, which is affected by the shear strength. Ermolaev et al. [18] studied the effect of small angles of attack on the transition from laminar to turbulent flow on swept wings at different Mach numbers using a T-325 wind tunnel. Milinović et al. [19] simulated supersonic and subsonic integral flight speed and rotational damping data based on wind tunnel tests and calculated aerodynamic coefficients. Lopez et al. [20] experimentally verified a simplified model of a wind turbine blade using aluminum beams of different geometries in a wind tunnel test, and studied the instability of nonlinear behavior caused by large deflections. Akbıyık et al. [21] analyzed the two- and three-dimensional flow structures and the induced flow effects generated by the plasma actuator in wind tunnel tests with a Reynolds number of 4.8×10^{4}.

Due to the influence of unsteady flow in the test chamber, it is difficult for the supersonic jet to achieve the ideal expansion state (pressure on both sides of the nozzle exit section is equal) as expected. When approaching the ideal expansion state, the supersonic jet will constantly change between under-expansion and over-expansion at the nozzle exit, and the core area of the jet will experience alternating shock waves and expansion waves, resulting in strong pressure fluctuations in the central flow field.

This study employs RANS and DNS methods to carry out steady and unsteady numerical simulations to study the back pressure matching relationship of the supersonic jet field in the test chamber. Under the conditions of the total pressure P_{in} at the inlet of the wind tunnel nozzle and the Mach number Ma_0 of the test chamber jet, the static pressure P_{out} at the outlet of the wind tunnel is adjusted the static pressure P_{out} at the wind tunnel outlet, the jet at the nozzle outlet is in an ideal expansion state, and a Mach number-height-uniform airflow is generated in the core region of the jet. Furthermore, the flow field characteristics of the supersonic jet in the limited space of the research test chamber were studied, and the development and instability of the shear layer of the supersonic jet, the interference of vortices and collectors, and the large-scale spatial vortex structure were characterized.

2 METHODS AND MATERIALS

2.1 Calculation Method Optimization

The fluid generated by the supersonic wind tunnel is turbulent, and it has the characteristics of diffusion, dissipation, randomness and vortex. The mainstream numerical simulation methods are divided into RANS, DNS, and large Eddy simulation (LES). RANS solves the uniform flow field and has a wealth of turbulence models for different types of flow. Its grid is Reynolds number independent and can better predict the flow trend of the flow field.

When calculating the steady-state flow field of a jet using the RANS method, there are usually five turbulence models to choose from, namely standard k–ε, RNG k–ε, realizable k–ε, standard k–ω and SST k–ω. Balabel et al. [22] used the above five turbulence models to numerically simulate the flow field of supersonic jets. The results show that the SST k–ω model performs best in the simulation of the flow field of supersonic jets, and the results of this model are basically consistent with the measured values. The SST k-ω model takes into account the influence of turbulent shear stress on the calculation results, and the turbulent viscosity formula is modified, which improves the calculation accuracy of the supersonic jet flow field.

To fully understand the development of the jet shear layer, instability, and vortex shedding in the wind tunnel test chamber under supersonic conditions, and to determine the flow characteristics of the supersonic jet field, this paper uses DNS to perform transient calculations of the supersonic jet flow field.

2.2 Numerical Simulation Model

The model of the wind tunnel test chamber is shown in Fig. 1. It is mainly composed of a Laval nozzle, a test chamber, a collector, and an outlet conduit [23]. The test chamber platform is equipped with a measuring probe to be tested in the wind tunnel test. After the gas is compressed and accelerated by the Laval nozzle, it forms a supersonic jet, which flows into the test chamber through the nozzle outlet and finally flows out through the collector connected to the outlet conduit.

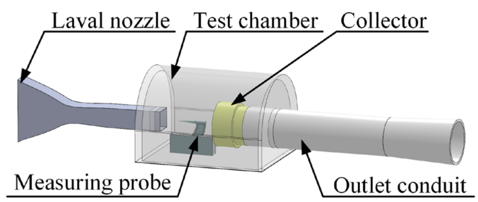

Fig. 1. Schematic diagram of the wind tunnel model

The flow field of the wind tunnel test model is shown in Fig. 2. The numerical calculation object is the total pressure $P_{in}=180$ kPa at the nozzle inlet. By adjusting the static pressure P_{out} at the wind tunnel outlet, the Mach number at the nozzle outlet is Mach 1.5 and the nozzle outlet jet is in an ideal expansion state of supersonic flow. The nozzle outlet is a matrix with a side length of 2000 mm, and the axial computational domain length is 79500 mm. The inlet of the Laval nozzle is given as the pressure inlet boundary, the outlet of the wind tunnel is the pressure outlet, and the boundary conditions for the remaining surfaces are insulated non-slip walls.

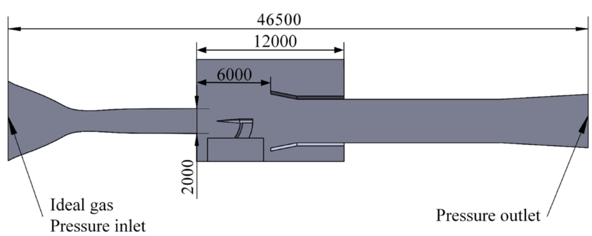

Fig. 2. Jet computational domain dimensions and boundary conditions (central cross-section of the fluid domain) (in mm)

The section from the nozzle outlet to the test stylus is the core of the jet field in the test chamber. When achieving back pressure matching for a given jet Mach number, the Mach number at the nozzle outlet should be the main assessment object to ensure that the Mach number at the typical position on the centerline of the nozzle outlet jet is stable. Therefore, reasonable Mach number monitoring points should be set in the core area of the jet field to obtain the velocity distribution at typical locations. As shown in Fig. 3, the coordinates of the center point of the nozzle outlet section (0, 0, 0) are taken as the origin of coordinates. Five evenly distributed Mach number monitoring points P1 to P5 are set on the axis of the nozzle outlet in the core region of the jet field, of which monitoring point P1 is set at the origin of coordinates and monitoring point P5 is set at the tip of the probe. Table 1 demonstrates the specific coordinates of the five monitoring points.

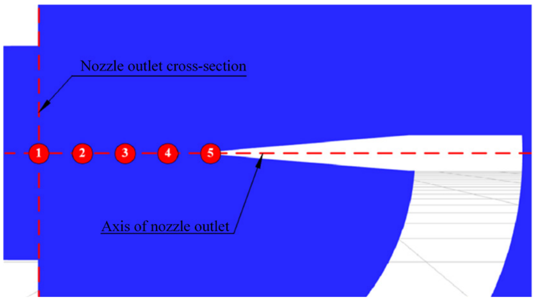

Fig. 3. Schematic diagram of the monitoring point on the axis of the nozzle outlet

Table 1. Coordinate data of the axis monitoring points

Point number	P1	P2	P3	P4	P5
X-coordinate [mm]	0	400	800	1200	1600
Y-coordinate [mm]	0	0	0	0	0
Z-coordinate [mm]	0	0	0	0	0

2.3 Back Pressure Matching Method

For the steady-state flow field simulation analysis of supersonic jets, the ideal expansion state of the jet at the nozzle outlet is required for pressure matching. A slight deviation in the back pressure can cause the jet state to deviate. Through a large number of back pressure matching simulation calculations, the Mach number distribution of the jet centerline from the nozzle outlet to the measuring probe satisfies the given supersonic Mach number, and summarizes the characteristics of the jet field structure and the distribution of flow parameters in the core region under typical non-matching parameters.

2.3.1 Numerical Simulation Parameter Optimization

The supersonic jet process is a compressible flow, and the ideal-gas model should be used for numerical simulation. The k–ω SST turbulence model is used to solve and turn on the energy equation. The density-based solver needs to be preprocessed to overcome the singularity of the system matrix in the low Mach number flow region. The pressure-based solver is good at capturing the physical characteristics of the jet flow field. For high-speed compressible flows, it is suitable to solve the energy and momentum equations by coupled method, which helps the numerical simulation to converge. The spatial discretization method for pressure is set to Second Order, which is suitable for compressible flow. Supersonic jets are often accompanied by the generation of shock waves. The default settings for other spatial discretization methods such as density and momentum are first-order upwind schemes. However, this format will smooth out the shock waves in compressible flows. Therefore, the density, momentum, and other spatial discretization methods are changed to the quadratic upwind interpolation (QUICK) format to make the calculation results more accurate.

The numerical simulation monitors the residuals of each equation to estimate the convergence of the calculation. When the residual of the energy equation drops to 1×10^{-6} and the residuals of other equations such as the continuity equation and velocity equation drop to 1×10^{-3}, the numerical simulation program will converge by default. The residual calculation value is only a general method for roughly judging whether the calculation has converged. According to the law of conservation of mass, the mass flow rate values at the inlet and outlet of the nozzle should be the same. Therefore, the mass flow rate difference between the inlet boundary and the outlet boundary is monitored. When the residual of the monitored mass flow reaches 1×10^{-8}, it can be judged that the steady-state numerical simulation has reached a converged state.

2.3.2 Mesh Construction and Mesh-Independent Verification

The jet computational domain is discretized using a combination of hexahedral and polyhedral meshes, which ensures that the entire computational domain mesh is structured and effectively improves the mesh quality. To more accurately study and analyze the flow field in the core region of the supersonic jet in the wind tunnel, the mesh of the Laval nozzle as a whole and the core region of the jet from the nozzle outlet to the collector was densified; the boundary layer was added to the probe and the collector wall.

As shown in Fig. 4, when the fluid flow state is fully developed turbulence, the turbulent flow near the flat wall can be divided into three regions. At the near wall, the viscous force is dominant because the inertial force is small compared to the viscous force. The fluid velocity in this region varies linearly with the distance from the wall, exhibiting laminar flow. This region is the viscous sublayer. When the flow begins to transition to turbulence, the area away from the wall is called the buffer layer, and eventually, when the flow completely transitions to a turbulent state, it is called the turbulent core.

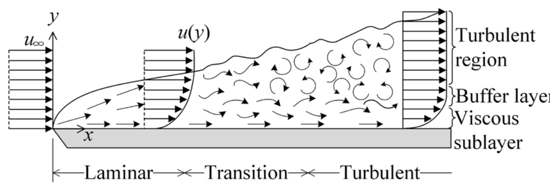

Fig. 4. Schematic diagram of fluid flow state

For the study of turbulent boundary layers, von Karman derived a logarithmic law based on the Prandtl mixing length theory using a dimensional analysis method, further subdivided the turbulent boundary layer into four regions: the viscous sublayer ($0<y^+<5$), the buffer layer ($5<y^+<30$), the log-law region ($y^+>30$), and the outer layer, as shown in Fig. 5. The boundary layer is usually defined by the two dimensionless physical quantities u^+ and y^+, which are defined as follows:

$$u^+ = \frac{u}{u^*}, \tag{1}$$

where u^+ represents the dimensionless velocity, u represents the fluid velocity in the boundary layer, and u^* is the friction velocity near the wall surface, which is defined as follows:

$$u^* = \sqrt{\frac{\tau_\omega}{\rho}}, \tag{2}$$

where τ_ω is the shear stress on the wall surface, y^+ represents the dimensionless distance to the wall, y represents the distance from a point in the boundary layer to the wall, and

ν represents the kinematic viscosity of the fluid [m²/s]. Therefore, after determining y^+ at the first layer of the wall, the first layer spacing can be calculated.,

$$y^+ = \frac{u^* y}{\nu}. \tag{3}$$

For viscous bottom layers ($0<y^+<5$), the viscous force is linearly related to the velocity gradient; for the fully turbulent layer, u^+ and y^+ are approximately logarithmically related, which is called the logarithmic law layer; for the buffer layer, the linear relationship curve and the logarithmic law curve intersect in the buffer layer, and the y^+ value corresponding to the intersection point is around 11.

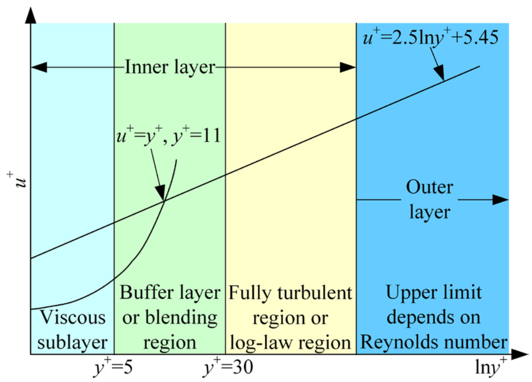

Fig. 5. Turbulent boundary layer region division

For the k–ω SST turbulence model used in this paper, the wall function is not used to solve the distribution of physical quantities in the viscous sublayer and buffer layer. Instead, the NS equation is discretized and solved throughout the basin, so the first layer of the boundary layer grid should be in the viscous sublayer. Taking $y^+=1$, the first mesh layer thickness is calculated to be 0.07 mm. The model includes a total of 18 million mesh cells, with a minimum cell size of 6 mm and a minimum orthogonal quality of 0.144.

The Mesh-independent verification is used to explore the impact of the number of mesh cells on the accuracy of the numerical simulation, so as to select an appropriate number of mesh cells to ensure the accuracy of the numerical simulation. Under the condition of ensuring that the computational domain model of the wind tunnel jet field is exactly the same, the mesh size of the entire nozzle and the shear layer in the test chamber (from the nozzle outlet to the collector area) is adjusted by adjusting the global size of the mesh. Three different mesh models with 16 million, 18 million and 20 million mesh elements are set up, and the minimum mesh element size is 6.5 mm, 6 mm and 5.5 mm, respectively. After meshing, the mesh quality is checked to ensure that a high-quality mesh model is output. The minimum orthogonal quality of the mesh is an important criterion for measuring the quality of the mesh. It represents the deviation of the shape of the representative element from the ideal orthogonal shape. In the case of adding a boundary layer to the fluid domain mesh, the minimum orthogonal quality should generally be greater than 0.1. Table 2 shows the results of the mesh quality check for the three types of jet field meshes described above.

Table 2. Mesh quality test results

Mesh cells in million	16	18	20
Minimum cell size [mm]	6.5	6	5.5
Minimum orthogonal mass	0.128	0.144	0.151

The results of the mesh quality test show that the meshes of the three sizes have high mesh quality. The steady-state flow field of the supersonic jet is calculated under the same conditions, where the static pressure at the outlet P_{out} is set to 92 kPa. The comparison of the Mach number calculation results and the calculation error at the P1-P5 monitoring points are shown in Figs. 6-10.

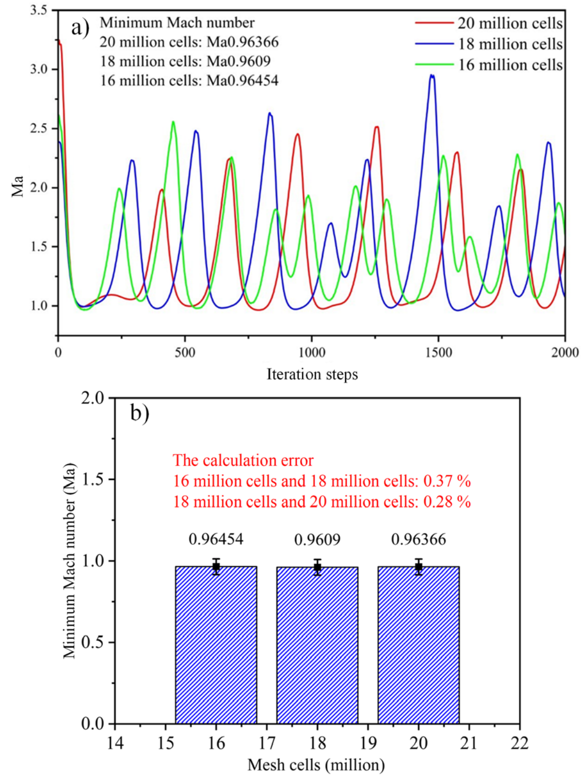

Fig. 6. P1 monitoring point independence verification;
a) minimum Mach number at P1, and b) calculation error at P1

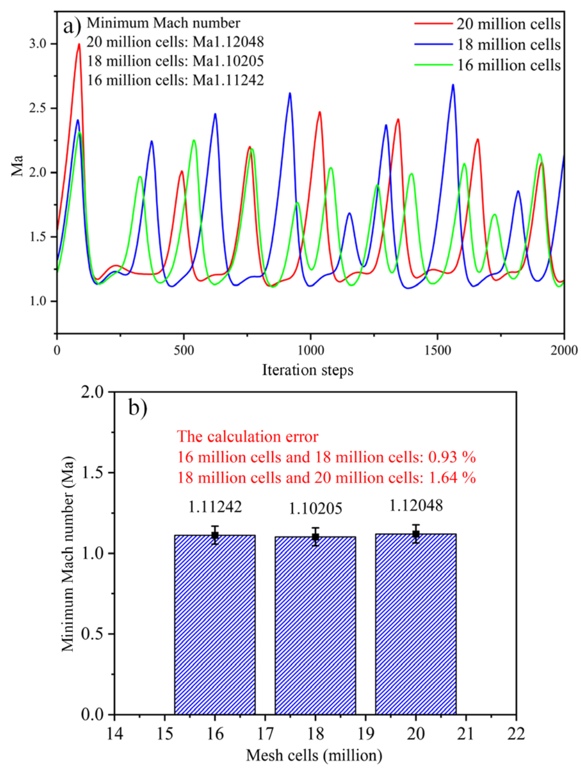

Fig. 7. P2 monitoring point independence verification;
a) minimum Mach number at P2, and b) calculation error at P2

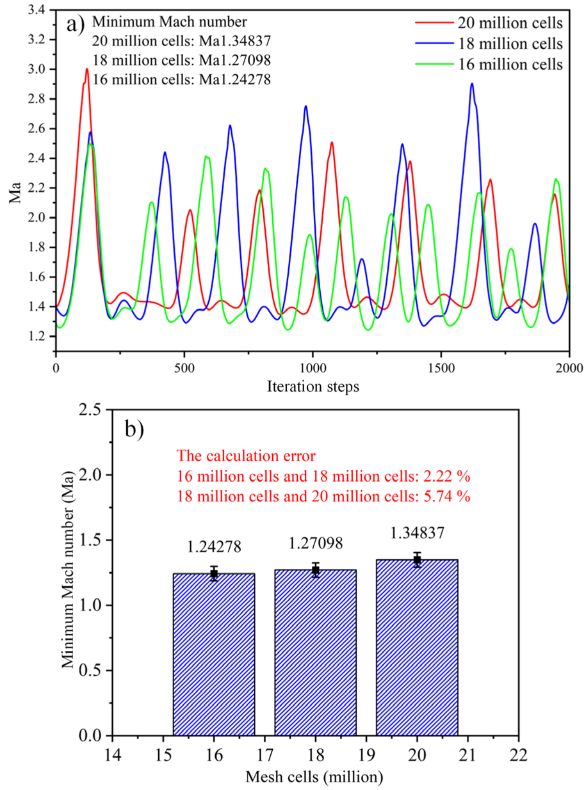

Fig. 8. P3 monitoring point independence verification; a) minimum Mach number at P3, and b) calculation error at P3

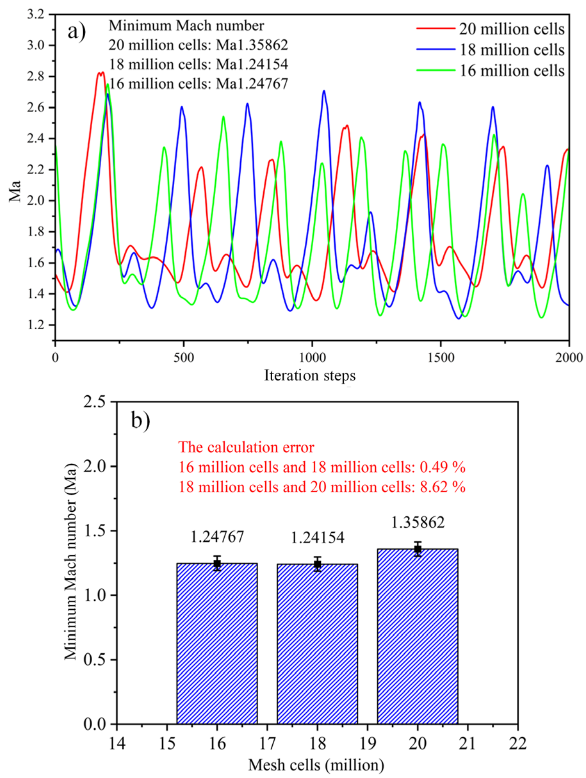

Fig. 9. P4 monitoring point independence verification; a) minimum Mach number at P4, and b) calculation error at P4

From Figs. 6-10, it can be seen that for the five monitoring points (P1-P5) set in the core area of the jet from the nozzle outlet to the probe section, each point shows a regular fluctuation state. Taking the minimum Mach number in the iteration of the axis monitoring points P1-P5 as the reference basis, the number of mesh cells increases from 16 million to 18 million, 20 million, and the minimum Mach number error values are all within 10 %. The impact of reducing the mesh size on the calculation results is negligible. The specific error values are shown in Table 3. The verification conditions for mesh independence are met, indicating that the calculation accuracy of 18 million mesh cells can meet the calculation requirements.

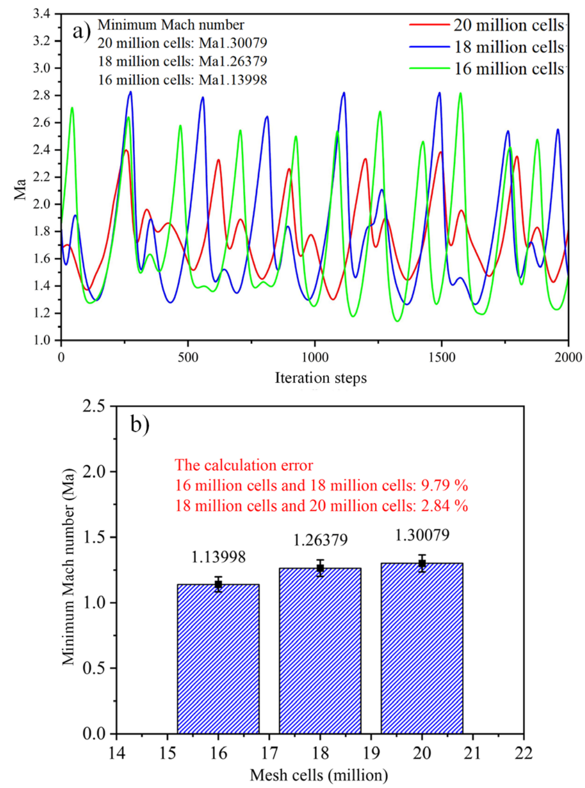

Fig. 10. P5 monitoring point independence verification; a) minimum Mach number at P5, and b) calculation error at P5

Table 3. Mesh comparison error table

Point number	Mesh cells comparison	Error [%]
P1	16 and 18 million	0.37
	18 and 20 million	0.28
P2	16 and 18 million	0.93
	18 and 20 million	1.64
P3	16 and 18 million	2.22
	18 and 20 million	5.74
P4	16 and 18 million	0.49
	18 and 20 million	8.62
P5	16 and 18 million	9.79
	18 and 20 million	2.84

2.3.3 Propose a Back-Pressure Quick Matching Method

Propose back-pressure matching basis

The purpose of supersonic jet back pressure matching is to keep the total pressure P_{in} at the entrance of the wind tunnel constant at 180 kPa, and to adjust the static pressure P_{out} at the outlet of the wind tunnel so that the pressure at the outlet of the nozzle is consistent with the working environment pressure (atmospheric pressure). the

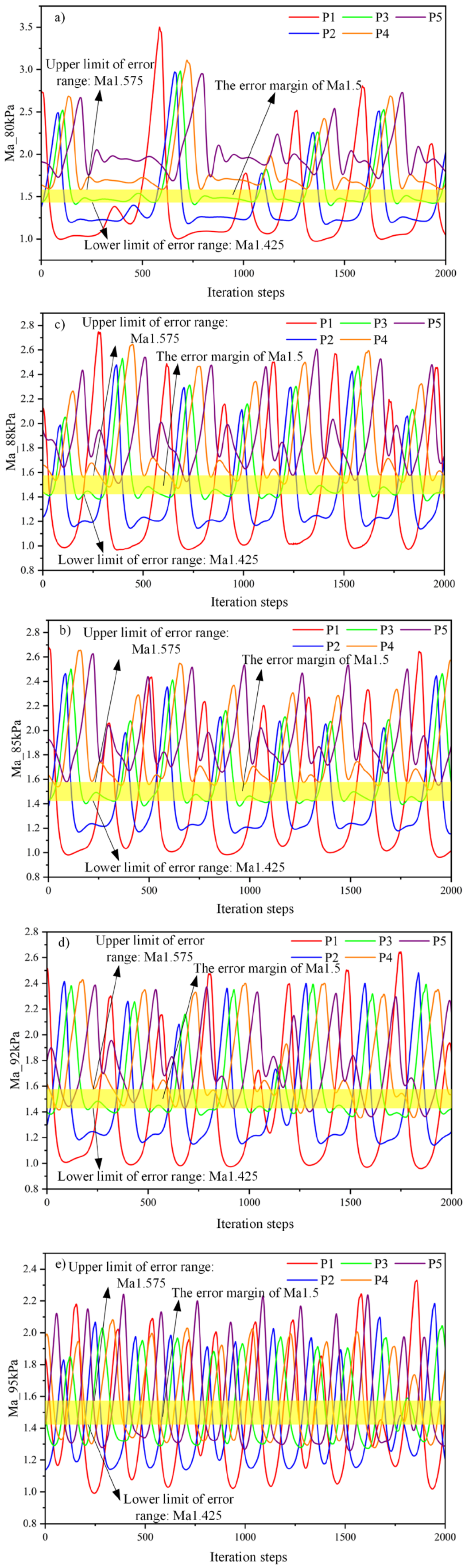

Fig. 11. Mach number at the axis monitoring point for different outlet pressures; a) P_{out} = 80 kPa, b) P_{out} = 85 kPa, c) P_{out} = 88 kPa, d) P_{out} = 92 kPa, e) P_{out} = 95 kPa

supersonic fluid ejected from the nozzle outlet is in an ideal expansion state, achieving a stable Mach number in the core area of the jet from the nozzle outlet to the probe section in the chamber. At this time, the static pressure at the wind tunnel outlet is the standard static pressure P_m for achieving wind tunnel jet back pressure matching.

Under ideal expansion conditions, a supersonic jet with a Mach 1.5 is ejected from the outlet of the Laval nozzle of this standard profile. The Mach number at the nozzle outlet is the main research object, and a steady-state numerical simulation is conducted on the 18 million cells. When the Mach number deviation at the typical position of the centerline of the nozzle jet does not exceed 5 %, the static pressure P_{out} at the outlet of the wind tunnel is the matching value of the back pressure P_m.

When the jet field simulation calculation converges, the number of iterations at convergence is recorded as S_0, which means that when the calculation is iterated to S_0, the residual values and mass flow rates have met the convergence conditions. Therefore, the solution results at any iteration step after S_0 can meet the actual flow field distribution under this working condition. Take the calculation result of the outlet pressure P_{out} of 92 kPa as an example Fig. 11a) shows the Mach number of the P1-P5 monitoring points after the S_0 and the change of the number of iterations. (2000 iterations are selected.) This means that the Mach number of the P1-P5 monitoring points at each iteration in the figure is the Mach number distribution of the actual jet field under the working condition. Fig. 11. shows the Mach number curves of the P1-P5 monitoring points after the convergence iteration step S_0 under the conditions of outlet pressures P_{out} of 80 kPa, 85 kPa, 88 kPa, and 95 kPa, respectively.

Rapid backpressure matching process

Step 1. Calculate and obtain the Mach number fluctuation curve of the measurement point that meets the error requirements. For example, the outlet speed of this type of Laval nozzle under standard ideal expansion conditions is Mach 1.5, so the curve of the monitoring point Mach number within 5 % of the calculated error (i.e. Mach 1.425 to 1.575) is selected.

Step 2. Since the Mach number changes at each monitoring point have obvious periodicity, in order to facilitate observation and statistics, the 500-step partial curve of the Mach number calculation process at each monitoring point under the above-mentioned P_{out} conditions is intercepted for study, and it should be ensured that the intercepted part contains the complete cycle of the Mach number change at the monitoring point, as shown in Figs. 12-16.

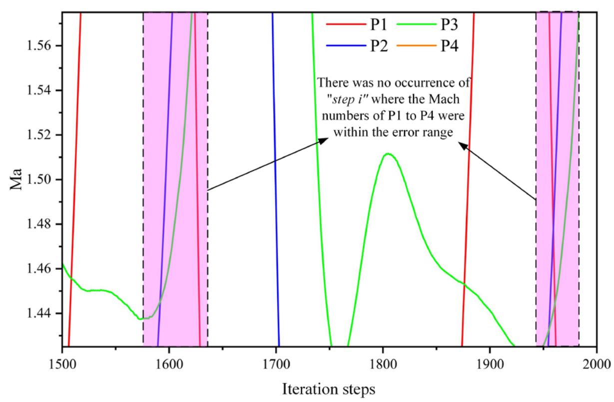

Fig. 12. Curve processing at an outlet pressure of 80 kPa

Step 3. Determine whether the Mach number fluctuation curve of a calculation step is within the error range. The P5 is at the tip of the measuring probe, and the flow field fluctuates greatly due to the influence of the measuring probe. The data analysis only takes

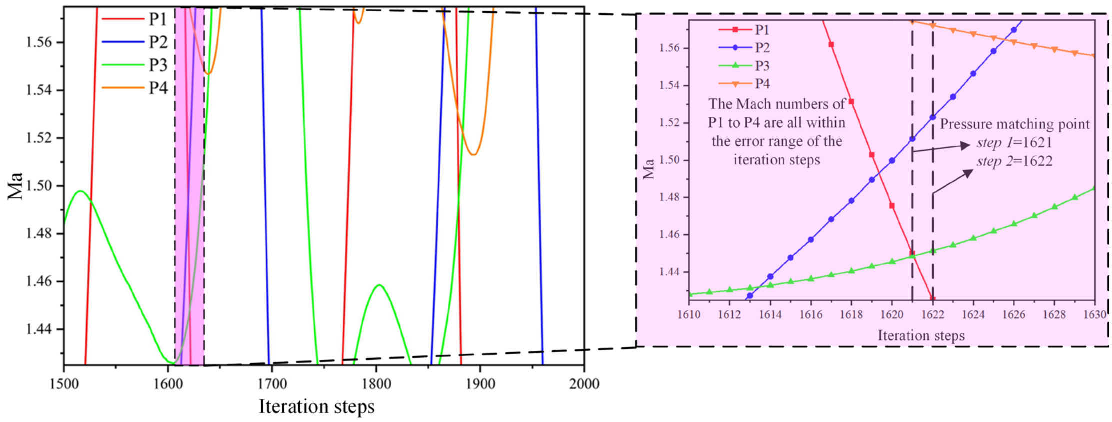

Fig. 13. Curve processing when back pressure matching is satisfied with an outlet pressure of 85 kPa

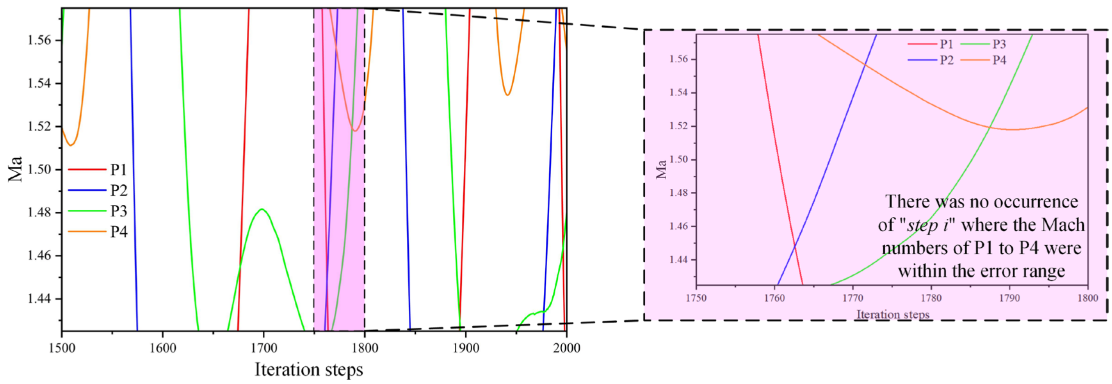

Fig. 14. Curve processing at an outlet pressure of 88 kPa

the key positions of the axial monitoring points P1-P4 as the basis for back pressure matching. When a certain iteration number step i exists in the intercepted partial curve, and the Mach number curve of the P1-P4 monitoring points at *step i* also exists in the Mach 1.425 to 1.575 curve, it means that the Mach number distribution on the centerline of the jet from the nozzle outlet to the probe at *step i* is uniform and within the error range of the standard Mach number of 1.5 when the back pressure is matched. The simulation results for this *step i* are the jet field distribution that satisfies the wind tunnel jet back pressure matching conditions. The set wind tunnel outlet pressure P_{out} is the solution P_m for matching the back pressure of the supersonic wind tunnel jet.

The specific processing results of the Mach number curves at the monitoring points with the outlet pressures P_{out} set to 80 kPa, 85 kPa, 88 kPa, 92 kPa, and 95 kPa are shown in the Figs. 12-16.

1. P_{out} = 80 kPa

As shown in Fig. 12, within the standard Mach number of 1.5 error range (Mach 1.425 to 1.575), there is no solution that satisfies the back pressure matching conditions at monitoring points P1-P4 during the calculation process, that is, there is no iteration step *step i* in the figure that makes the curves shown at P1-P4 all fall between Mach 1.425 to 1.575 at *step i*, thus not meeting the conditions for matching the back pressure of the wind tunnel jet.

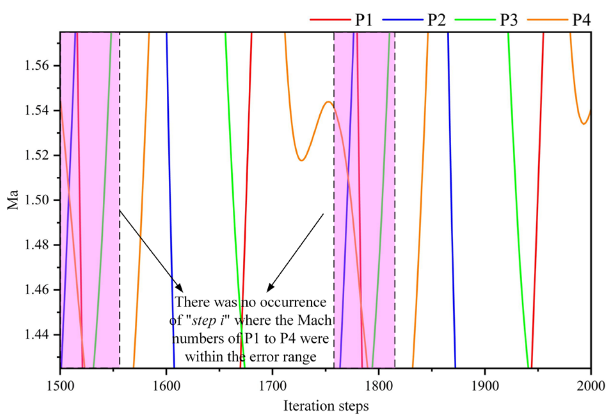

Fig. 15. Curve processing at an outlet pressure of 92 kPa

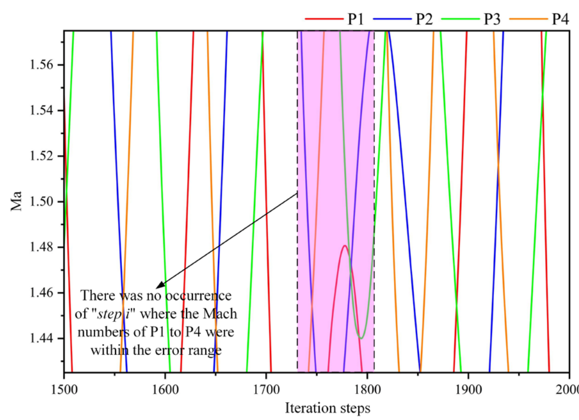

Fig. 16. Curve processing at an outlet pressure of 95 kPa

2. P_{out} = 85 kPa

As shown in Fig. 13, when the outlet pressure P_{out} = 85 kPa, there are two solutions that satisfy the back pressure matching in the Mach number curve during the iteration process: step 1621 and step 1622. That is, *step 1* = 1621, *step 2* = 1622. When the iteration reaches *step 1* and *step 2*, the Mach numbers of the P1-P4 are all within the range of Mach 1.425-1.575. At this time, the velocity distribution of the core area of the jet from the nozzle outlet to the probe section is stable, achieving back pressure matching of the wind tunnel jet.

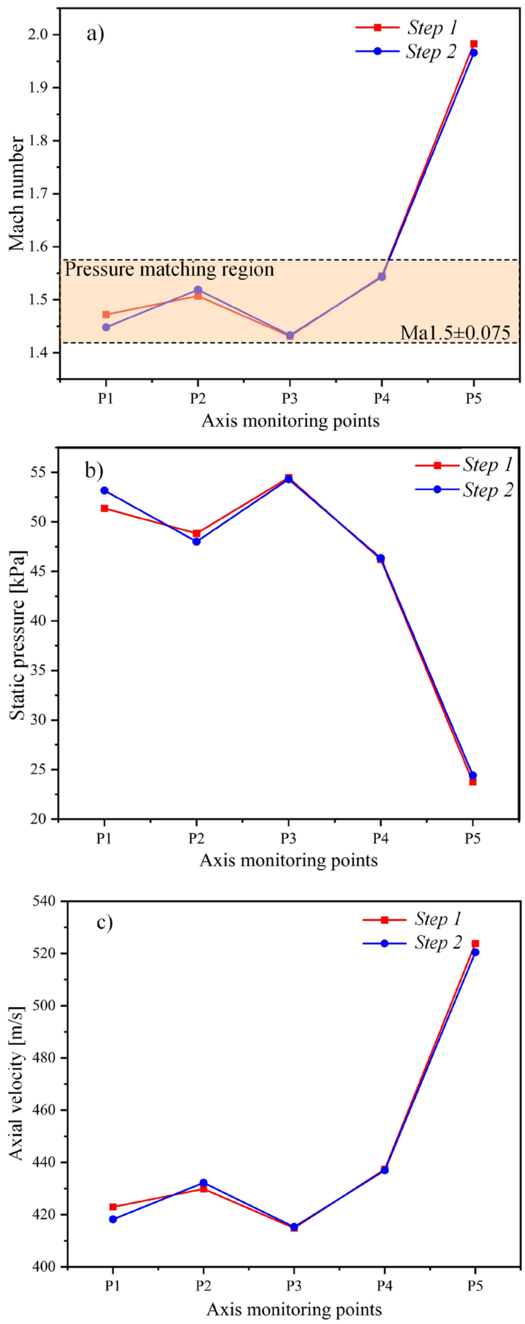

Fig. 17. Distribution of key physical parameters of the axis under back pressure matching conditions; a) Mach number distribution at monitoring points, b) static pressure distribution at monitoring points, and c) axial velocity distribution at monitoring

3. P_{out} = 88 kPa

As can be seen from Fig. 14, there is no solution for back pressure matching at an outlet pressure of 88 kPa, i.e. there is no iteration number *step i* in the graph such that the curves shown by P1-P4 are simultaneously between Mach 1.425 and 1.575 at *step i*, thus not meeting the conditions for back pressure matching of the wind tunnel jet.

4. P_{out} = 92 kPa

As can be seen on Fig. 15, there is no solution for back pressure matching at an outlet pressure of 92 kPa.

5. P_{out} = 95 kPa

As can be seen on Fig. 16, no solution for back pressure matching is found for an outlet pressure of 95 kPa.

In summary, the ideal outlet pressure P_m = 85 kPa is achieved when the back pressure matching conditions of the wind tunnel are satisfied. At this time, the jet at the outlet of the nozzle is in an ideal expansion state, and the Mach number of the centerline of the jet in the cabin is stable at Mach 1.5.

Characteristics of the distribution of the axis of the nozzle jet at the back pressure matching point

Extract the data on the Mach numbers of monitoring points P1-P5 at step 1 and step 2 of the numerical simulation results under the operating condition of P_m = 85 kPa, as shown in Table 4.

Fig. 17a shows the Mach number distribution of monitoring points P1-P5 when back pressure matching is achieved. It is evident that the Mach number distribution on the centerline of the nozzle outlet jet fluctuates periodically within the Mach 1.5 error range, which can provide the supersonic jet at the desired expansion state of the nozzle outlet. The flow field near the tip of the P5 probe is highly turbulent, and the presence of the probe will greatly increase the Mach number, so it is not representative in the study. Figs. 17b and c show the static pressure and axial velocity distributions at monitoring points. It can be seen that the key physical parameters of the jet field from the outlet of the nozzle to the stylus are distributed stably, which further verifies the back pressure matching method described above.

Table 4. Mach number at monitoring points under back pressure matching condition

Point number	Mach number		Axial velocity [m/s]		Static pressure [kPa]	
	step 1	step 2	step 1	step 2	step 1	step 2
P1	1.472	1.448	422.975	418.239	51.37	53.17
P2	1.507	1.519	429.881	432.249	48.84	48.01
P3	1.431	1.433	414.885	415.279	54.47	54.31
P4	1.545	1.543	437.379	436.985	46.21	46.34
P5	1.983	1.966	523.805	520.451	23.77	24.43

Back pressure matching results and verification

The flow field analysis was performed using the steady-state simulation results of the wind tunnel jet field in *step 1*. Fig. 18 shows the Mach number, static pressure, and pathlines diagram of the core area of the jet (from the nozzle outlet to the collector inlet) in the central plane of the wind tunnel test chamber (Z = 0 mm) under the wind tunnel back pressure matching condition.

The numerical simulation results of the above back pressure matching working conditions can analyze and summarize the flow field characteristics of the ideal expansion state of the nozzle jet and the influence of the equipment in the test chamber, such as the probe, test bench, and collector, on the jet field. At this time, the static pressure at the nozzle outlet is equal to the static pressure in the test chamber, and the supersonic jet injected into the wind tunnel test chamber is in an ideal expansion state. As shown in the A1, B1, and C1 areas in Fig. 18, the core area of the jet from the nozzle outlet to the probe section, the supersonic jet in the ideal expansion state has a relatively uniform flow within the jet boundary, and the jet boundary is stable. At this time, there is no repeated phenomenon of accelerated expansion and decelerated compression, which makes the range of the uniform jet zone break through the limitation of the rhombus zone in the traditional high-speed free jet wind tunnel during supersonic speed tests. The physical parameters such as the Mach number and static pressure in the core of the jet are uniform and stable. The jet trajectory is stable, and the supersonic jet flows steadily in the horizontal direction without significant airflow deviation, providing good simulation conditions for wind tunnel tests.

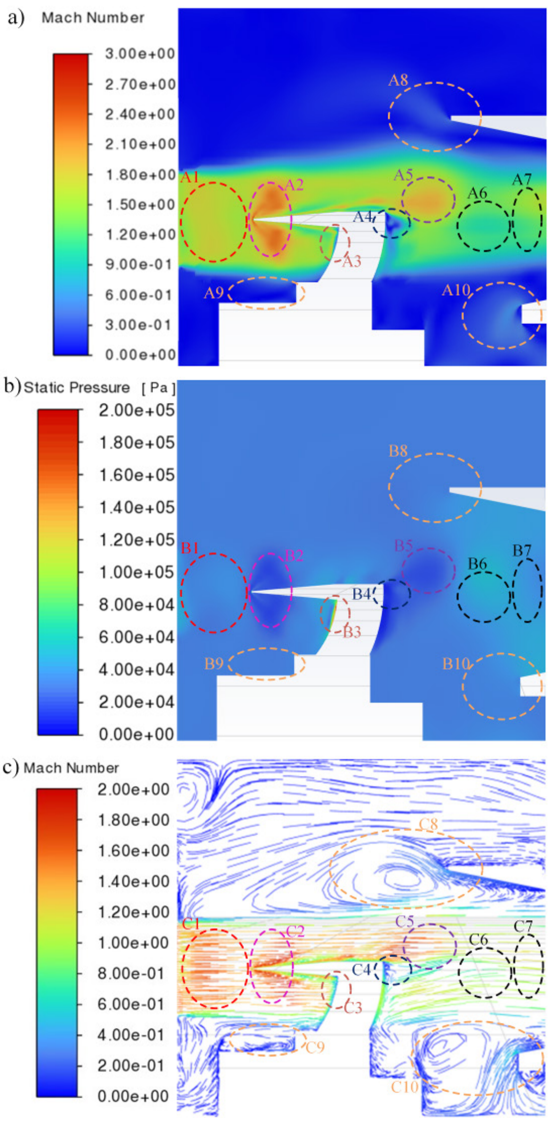

Fig. 18. Flow field at the center plane under back pressure matching conditions (P_{out} = 85 kPa); a) Mach number contour, b) static pressure contour, c) pathlines diagram

There is a clear concentration of the velocity in the A2, B2, and C2 regions in Fig. 18. The reason is that after the uniform and stable supersonic jet is ejected from the nozzle into the test chamber under ideal expansion conditions, the jet flows through the probe and is blocked by the probe, as shown in the C2 region It is evident that the blocked supersonic jet will flow along the surface of the conical probe. Under the condition of constant flow rate, the cross-sectional area of the jet is reduced due to the influence of the probe, resulting in an increase in the flow velocity and a decrease in the pressure in this area, so that the tip of the probe has a higher Mach number.

Unlike the above-mentioned increase in flow velocity due to the decrease in the cross-sectional area of the basin at the tip of the probe, the jet Mach number at point A3 in Fig. 18 demonstrates a very significant decrease. The reason for this is that the arc test stand of the probe device at this point has a larger gradient on the windward side than the conical probe mentioned above. Line flow situation shows that the jet flow to the arc test frame can not flow smoothly along the surface of the mechanism, but is hindered by the arc test frame, causing the flow to be blocked and slowed down, so the Mach number in the A3 area is reduced. The deceleration of the jet flow in this area causes the air flow to gather, causing the pressure to rise, as shown in the B3 area in Fig. 18.

After the jet flows through the test bench, the central area of the jet is blocked by the probe mechanism, and only a small amount of fluid passes through the area C4 in the pathlines diagram in Fig. 18c, resulting in a lower static pressure at point B4 compared to the surrounding static pressure, forming a low static pressure area as shown in Fig. 18b, and also resulting in a lower fluid velocity in this area, forming a low Mach number area A4 in the Mach number cloud diagram in Fig. 18a. When the jet passes completely through the test bench device, the fluid, which was previously decelerated, is briefly accelerated by the obstruction of the probe mechanism, as shown in the A5 area, producing a clearly high Mach number region. The increase in fluid is also reflected in the decrease in static pressure in the B5 area. At the same time, it can be seen from the pathlines diagram in the C6 area that after the supersonic jet flows through the probe mechanism, the blocked jet produces fluid separation in this area. The fluid flowing through the C6 area is less likely to form a low Mach number region at A6. As can be seen from the A7, B7, C7, the jet area that has undergone a brief separation will once again be integrated, and the physical parameters such as Mach number and static pressure will then be distributed stably, forming a uniform and stable jet again, which then flows through the collector and is ejected from the wind tunnel outlet conduit.

The flow structure in the wind tunnel test chamber of the open-mouth device is complex and has high unsteadiness, as shown in the C8, C9, and C10 areas in Fig. 18. The vortices formed by vortex shedding in the supersonic jet shear layer continue to develop, become unstable, and evolve, and interfere with the collector at the rear end, forming fluid disturbances that will exacerbate the instability of the flow field. These include the large-scale pseudo-order vortex structure in the jet shear layer shown in C8, the large-scale spatial vortex structure induced by the jet shear layer and the low-speed fluid in the suction test chamber shown in C10, and the separation vortex structure in the corner of the test chamber shown in C9. The mutual interference, fusion, and development of these spatial vortex structures increase the complexity of the flow field structure of the test chamber and exacerbate the pulsating characteristics of the flow field.

This study also studies the flow field characteristics in the plane on both sides of the backpressure matching (Z = 700 mm, Z = –700 mm). The center plane of the test chamber (Z = 0 mm) is set as *Plane 1*, and the plane at Z = 700 mm in the test chamber is set as *Plane 2* to analyze the influence of the measuring probe on the jet field. Fig. 19 demonstrates the Mach number, static pressure and pathlines diagram of the fluid domain in *Plane 1* and *Plane 2*.

Since there is no test bench device in the *Plane 2* to interfere with the supersonic jet, the Mach number and static pressure zone of the E1 and G1 jet core flow field shown in Fig. 19b are more uniform and stable. The I1 region jet is in an ideal expansion state, and the fluid pathlines is ejected horizontally from the nozzle outlet. Additionally, the Mach number jump region in the E2 region caused by the tip of the measuring probe is significantly reduced, and the Mach number in the E2 region is similar to the Mach number of the surrounding flow field, both remaining near the standard Mach 1.5 at the nozzle outlet. The static pressure in the G2 area and the flow field pathlines in the I2 area in Fig. 19 can be compared with the flow fields in F2 and H2 in *Plane 1*. It is evident that the influence of the probe tip on the flow field is only in a small area near the tip, and the influence on the flow field in the outer area of the test bench is small. There is still a large range of Mach number mutation zones in the E3 region, indicating that the velocity concentration generated by the supersonic jet field flowing through the measuring probe in the outer region of the test bench still exists. The static pressure reduction region in the G3 region of the static pressure contour of *Plane 2* shown in Fig. 19d still exists, and the corresponding I3 region pathlines in the flow field pathlines diagram shown in Fig. 19f indicates that the jet fluid here has a significant acceleration process. This shows that the stepped shape of the test bench also has a more significant effect on the flow state of the jet field. After a short acceleration phase, the supersonic jet is re-integrated at the collector inlet. The flow field parameters are uniformly distributed in the E4, G4, and I4 areas of Fig. 19, and the jet field is again in a uniform and stable state, flowing through the collector and into the rear outlet conduit. It is worth noting that the separation of the flow field shown in Fig. 18 in the C4 region does not occur in the outer basin of the measuring probe, indicating that the separation of the flow field at the rear end of the measuring probe is caused by the blocking of the jet field by the measuring probe, and that this separation of the flow field only exists in the rear end of the measuring probe, and the effect on the flow field state of the core area of the jet is negligible. The spatial vortex structures shown in the E5 to E7, G5 to G7, and I5 to I7 regions of Fig. 19 still exist, indicating that the vortex structures generated by the shedding of the shear layer vortex of the supersonic jet have a significant impact on the flow field in the wind tunnel test chamber. The fluid disturbances caused by the collision of the spatial vortex structures with the collector and test bench device will make the unsteadiness of the flow structure in the wind tunnel test chamber more obvious.

This study summarizes and analyzes the characteristics of the jet field under typical non-matching parameters (P_{out} = 80 kPa, P_{out} = 88 kPa, P_{out} = 92 kPa, P_{out} = 95 kPa), and compares it with the standard jet field under the back pressure matching condition (P_m = 85 kPa). Characteristics were compared, and the flow field structure characteristics and core flow parameter distribution laws under non-matched parameters were studied. The Mach number contours, static pressure contours, and flow field pathlines diagram under different outlet pressures are shown in Figs. 20 to 22.

As shown in Fig. 20 above, when the inlet pressure P_{in} = 180 kPa is constant and the outlet pressure is less than the outlet operating pressure of 85 kPa, the pressure at the nozzle outlet is greater than the ambient pressure in the test chamber, and the supersonic jet in the wind tunnel test chamber is in an under-expansion state; when the outlet pressure is greater than the 85 kPa, the pressure at the nozzle outlet is less than the ambient pressure in the test chamber, and the supersonic jet in the wind tunnel test chamber is in an over-expansion state. The fluid in the state of under-expansion or over-expansion can cause alternating expansion and compression waves and wave interference at the center of the jet.

As shown in Fig. 20a, when the outlet pressure is low, the large pressure difference can cause the supersonic jet injected into the test chamber to continue accelerating in the core area, resulting in an under-expansion region with a high Mach number in the J1 region. Due to wave interference, the Mach number distribution in the J1 region will be uneven. When the uneven supersonic jet hits the test bench device in the under-expansion state, it also produces a large flow field mutation at the tip of the probe. Additionally, the range of the Mach number mutation zone J2 at the tip of the probe is significantly larger than the corresponding K2 mutation zone under the back pressure matching condition. The flow field distribution at the tip of the measuring probe is extremely uneven in the Mach number mutation zone, and a velocity concentration zone greater than Mach 3.0 is generated in the J4 zone. In addition, the supersonic jet in the J3 zone separates from the surface of the measuring probe, forming an unstable flow field with a large velocity gradient, which greatly reduces the flow field quality in the key flow field of the jet. This shows that the unstable under-expanded supersonic jet is more susceptible to the influence of the structure in the test chamber than the uniformly stable ideal expanded supersonic jet.

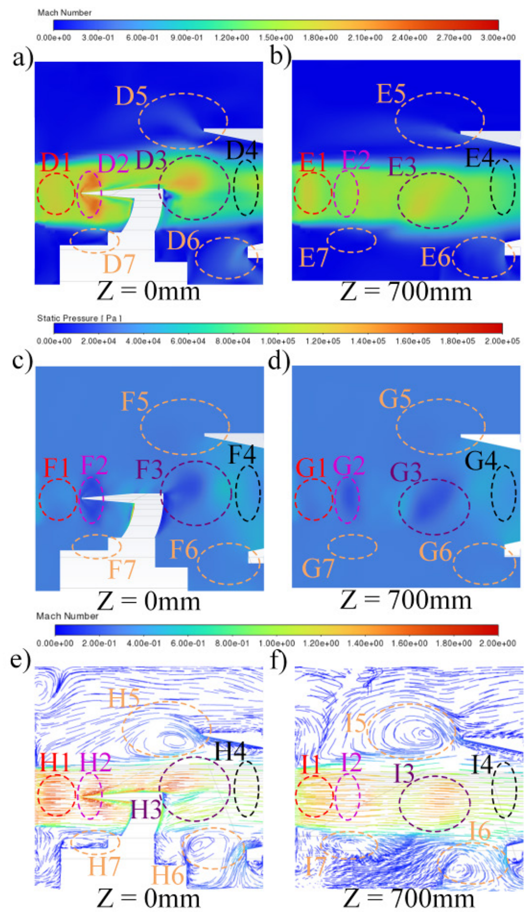

Fig. 19. Comparison of flow fields in different planes under back pressure matching conditions; a) Mach number contour of Plane 1, b) Mach number contour of Plane 2, c) static pressure contour of Plane 1, d) static pressure contour of Plane 2, e) flow field pathlines diagram of Plane 1, f) flow field pathlines diagram of Plane 2

As shown in the structure of the supersonic jet field in the over-expansion state in Figs. 20c, d, and f, the Mach number in the core area will continue to decrease compared to the ideal expansion state. At the same time, the phenomenon of alternating expansion and compression waves in the supersonic jet flow field during over-expansion will become more pronounced, inducing stronger pressure pulsations at the back of the core area. As shown by the flow fields in the L1, M1, and N1 areas of the figure, as the back pressure increases, the boundary between the acceleration and deceleration regions in the core of the jet becomes more distinct, which exacerbates the uneven distribution of the physical parameters of the jet flow field. As shown in L2, M2, and N2 in Fig. 20, when a periodic expansion wave flows through the test rig device, the unstable jet field will generate a large-scale Mach number sudden change area at the stylus. Under P_{out} = 88 kPa, a speed concentration caused by the instability of the jet shear layer appears in the L3 area.

Unlike the K4 region of the supersonic jet in the back pressure matching condition, which is re-integrated into a uniform and stable flow field, the flow field in the J6, L5, M4, and N4 regions in Fig. 20 shows that the fluid separation phenomenon still exists in the flow field at the rear end of the test chamber. The reason is that the flow field state of the under-expanded or over-expanded jet under back pressure mismatch is unstable, resulting in more drastic changes in the flow field structure after being disturbed by the test bench device, and then it is unable to re-rectify into a uniform and stable jet and spray into the collector.

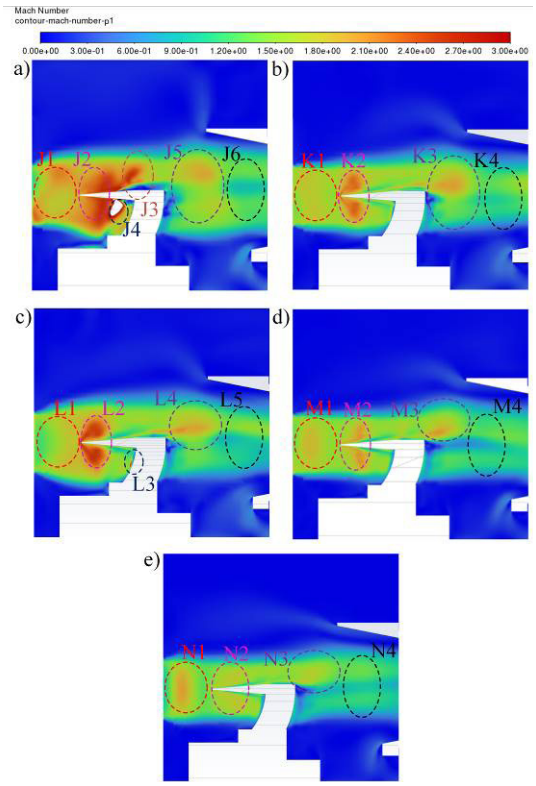

Fig. 20. **Comparison of Mach number of different back pressure jet fields;**
a) Mach number contour at P_{out} = 80 kPa, b) Mach number contour at P_{out} = 85 kPa,
c) Mach number contour at P_{out} = 88 kPa, d) Mach number contour at P_{out} = 92 kPa,
e) Mach number contour at Pout = 95 kPa

Fig. 21 shows the static pressure contours of the supersonic jet field at different outlet pressures of the wind tunnel. As shown in the O1 area in Fig. 21a, when the pressure at the outlet of the wind tunnel is low, the static pressure distribution in the core area of the jet is relatively chaotic, with obvious high static pressure areas, which will seriously affect the flow field quality of the supersonic jet. As shown in the Q1, R1, and S1 areas in the figure, when the pressure at the outlet of the wind tunnel is high, alternating high and low static pressure zones will appear in the core of the jet, and the greater the outlet pressure, the more obvious the boundary between the high and low static pressure zones. The expansion and compression waves that repeatedly appear are the main factors affecting the uniformity of the jet field. When an unstable jet under non-matching conditions collides with the stylus mechanism, a large low-static pressure area is formed at the tip of the stylus, as shown in the O2, Q2, R2, and S2 areas of the figure. It is worth noting that the jet field under various working conditions has obvious pressure concentration areas in the O3, P3, Q3, R3, and S3 regions, indicating that corners with large spatial gradients will affect the flow state of the fluid in a small area when they collide with supersonic jets.

After the supersonic jet passes through the test bench device under various working conditions, a significant low static pressure area appears in the O4, P4, Q4, R4, and S4 areas. This is because the supersonic jet undergoes a significant fluid acceleration process in this area, and the flow state of the jet field in the rear end area of the test bench changes significantly. Due to the interference of the test bench, the jet state becomes more unstable, which becomes the reason for the uneven static pressure distribution in the O5, Q5, R5, and S5 regions in the figure.

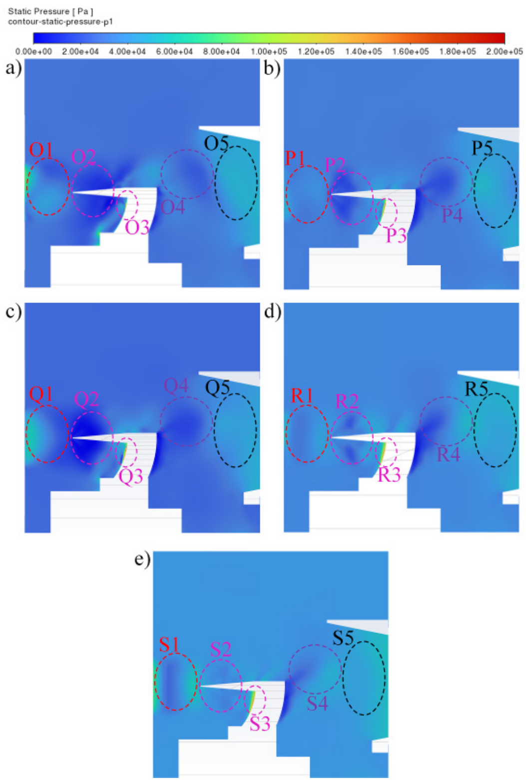

Fig. 21. **Comparison of the static pressure of the jet field with different back pressures;**
a) static pressure contour at P_{out} = 80 kPa, b) static pressure contour at P_{out} = 85 kPa,
c) static pressure contour at P_{out} = 88 kPa, d) static pressure contour at P_{out} = 92 kPa,
e) static pressure contour at P_{out} = 95 kPa

Fig. 22 shows the comparison of the flow field pathlines of the supersonic jet under different back pressures. For the flow in the core area U1 of the test chamber under the back pressure matching condition (P_{out} = 80 kPa), the fluid pathlines diagram are uniform and stable. There is no obvious disturbance in the field pathlines diagram in the core area, indicating that the supersonic jet is in an ideal expansion state. In a typical non-matching working condition, as shown in Fig. 22a, the jet in the under-expansion state has a significant expansion phenomenon in the core area T1 of the jet. The fluid pathlines of the shear layer of the jet gradually deviates from the axial direction and flows to both sides, indicating that the static pressure at the nozzle outlet under this working condition is greater than the ambient pressure in the test chamber. For the working conditions shown in Fig. 22 c, d, and e, the supersonic jet in the over-expansion state will alternate expansion and compression waves in the test chamber. The fluid traces in the core area of the jet shown by V1, W1, and X1 will repeatedly expand and compress, appearing to oscillate repeatedly near the axial direction. The shear layer of the supersonic jet in the non-matching working condition is extremely unstable. As shown in the figure, the jet traces in the V2, V3, W2, W3, X2, and X3 regions all show a flow field state in which the flow expands outwardly relative to the axial direction and then continues to compress inwardly.

For the supersonic jet in the under-expansion state shown in Fig. 22a, the fluid traces show a flow field state in which the flow expands outward. As shown in the figure T4, U3, V4, W4, and X4, in the rear section of the test chamber, the jet in the U3 area with matched back pressure is rearranged after passing through the test bench, and the flow field traces are once again stable, and then spray horizontally along the axial direction into the outlet pipe.

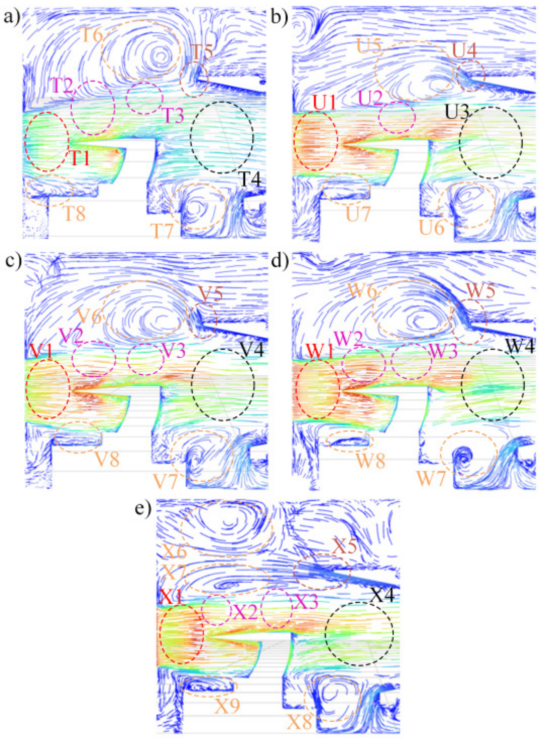

Fig. 22. Comparison of the jet field pathlines at different back pressures.
a) P_{out} = 80 kPa, b) P_{out} = 85 kPa, c) P_{out} = 88 kPa, d) P_{out} = 92 kPa, e) P_{out} = 95 kPa

As shown in the T5, U4, V5, W5, and X5 areas of Fig. 22, the jet shear layer and the collector interfere to produce obvious separation vortices in the test chamber. As the pressure at the outlet of the wind tunnel increases, the angle between the tangent line at the collector inlet and the axial direction of the separation vortex will gradually decrease. When the outlet pressure is too high, two large-scale space vortices appear in the X6 and X7 areas. The spatial vortex structure in the test chamber includes large-scale pseudo-ordered vortices in the jet shear layer, vortex structures generated by the jet shear layer being involved in the low-speed airflow in the test chamber, and the separation vortex structure in the spatial corners of the test bench and collector.

3 CONCLUSIONS

This study studies the conditions for generating an ideal expansion state jet in a supersonic wind tunnel with a standard Mach number of 1.5 at the nozzle outlet. A method for quickly obtaining the static operating pressure matching point of a supersonic jet is proposed, and the flow fields of an ideal expansion state jet and a supersonic jet under typical non-matching conditions are analyzed and compared. The research results show that:

1. When the Mach numbers of the monitoring points on the axis of the jet core are all within the Mach 1.5 error range of the standard nozzle exit, the supersonic jet is in an ideal expansion state. The exit pressure P_{out} under this operating condition is the solution P_m for supersonic wind tunnel back pressure matching.
2. The static pressure at the outlet of the wind tunnel nozzle under the back pressure matching condition (P_{out} = 80 kPa) is equal to the ambient pressure in the test chamber, and the physical parameters of the supersonic jet field are uniformly and stably distributed, which makes the range of the uniform jet zone break through the limit of the diamond-shaped zone. The jet has a uniform flow within the jet boundary, which improves the quality of the wind tunnel test jet flow field.
3. When the back pressure of the wind tunnel does not match, the supersonic jet will vary between under-expansion and over-expansion at the nozzle outlet. The core of the jet will experience alternating shock waves and expansion waves, resulting in strong pressure fluctuations in the central flow field, which will reduce the quality of the wind tunnel test jet flow field.

References

[1] Liu, Y., Sun, M., Liang, C., Cai, Z., Wang, Y. Structures of near-wall wakes subjected to a sonic jet in a supersonic crossflow. *Acta Astronaut* 151 886-892 (2018) **DOI:10.1016/j.actaastro.2018.07.048**

[2] Sun, M., Sandham, N.D., Hu, Z. Turbulence structures and statistics of a supersonic turbulent boundary layer subjected to concave surface curvature. *J Fluid Mech* 865 60-99 (2019) **DOI:10.1017/jfm.2019.19**

[3] Sabnis, K., Galbraith, D.S., Babinsky, H., Benek, J.A. Nozzle geometry effects on supersonic wind tunnel studies of shock-boundary-layer interactions. *Exp Fluids* 63 191 (2022) **DOI:10.1007/s00348-022-03543-1**

[4] Sandham, N.D., Reynolds, W.C. Three-dimensional simulations of large eddies in the compressible mixing layer. *J Fluid Mech* 224 133-158 (1991) **DOI:10.1017/S0022112091001684**

[5] Vreman, A.W., Sandham, N.D., Luo, K. Compressible mixing layer growth rate and turbulence characteristics. *J Fluid Mech* 320 235-258 (1996) **DOI:10.1017/S0022112096007525**

[6] Drozdov, S.M., Rtishcheva, A.S. Numerical investigation of air flow in a supersonic wind tunnel. *J Phys Conf Ser* 891 012043 (2017) **DOI:10.1088/1742-6596/891/1/012043**

[7] Lu, X.G., Yi, S.H., He, L., Gang, D.D., Niu, H.B. Experimental study on unsteady characteristics of shock and turbulent boundary layer interactions. *Fluid Dyn* 55 566-577 (2020) **DOI:10.1134/S0015462820030088**

[8] Lu, X.G., Gang, D.D., Niu, H.B., Zheng, W.P., Yi, S.H. Experimental investigation of hypersonic boundary layer transition on a 5° smooth straight cone. *Fluid Dyn* 57 1054-1064 (2022) **DOI:10.1134/S0015462822601139**

[9] Egorov, I.V., Duong, N.H., Nguyen, N.C., Palchekovskaya, N.V. (2022) Numerical simulation of the influence of a Mach wave on the laminar-turbulent transition in a supersonic boundary layer. *Dokl Phys* 67 144-147 **DOI:10.1134/S1028335822050019**

[10] Shen, J., Dong, J., Li, R., Zhang, J., Chen, X., Qin, Y., Ma, H. Integrated supersonic wind tunnel nozzle. *Chinese J Aeronaut* 32 2422-2432 (2019) **DOI:10.1016/j.cja.2019.07.005**

[11] Gounko, Y.P., Kavun, I.N. Peculiarities of the flows forming in processes of an impulse starting of a supersonic wind tunnel with different diffusers. *Thermophys Aeromech+* 26 195-214 (2019) **DOI:10.1134/S0869864319020045**

[12] Kosinov, A.D., Kocharin, V.L., Liverko, A.V., Semenov, A.N., Semionov, N.V., Smorodsky, B.V., Yatskikh, A.A. Effect of small angles of attack on turbulence generation in supersonic boundary layers on swept wings. *Fluid Dyn* 58 371-380 (2023) **DOI:10.1134/S0015462823600165**

[13] Yu, K., Xu, J., Liu, S., Zhang, X. Starting characteristics and phenomenon of a supersonic wind tunnel coupled with inlet model. *AerospSciTechnol* 77 626-637 (2018) **DOI:10.1016/j.ast.2018.03.050**

[14] Egorov, I.V., Nguyen, N.K., Pal'chekovskaya, N.V. Numerical simulation of the interaction of a Mach wave and a boundary layer on a flat plate. *High Temp+* 61 689-696 (2023) **DOI:10.1134/S0018151X23050036**

[15] Bottini, H., Paniagua, G., Schreivogel, P., Sonda, A., de las Heras, S. Design and qualification of a supersonic wind tunnel for induced boundary layer transition research. *P I Mech Eng G-J Aer* 229 562-578 (2015) **DOI:10.1177/0954410014537612**

[16] Wu, J., Liu, X., Radespiel, R. RANS simulations of a tandem nozzle supersonic wind tunnel. *AerospSci Technol* 49 215-224 (2016) **DOI:10.1016/j.ast.2015.11.041**

[17] Zhao, X.H., Yi, S.H., Mi, Q., Hu, Y.F., Ding, H.L. Skin friction reduction of hypersonic body by supersonic layer. *Fluid Dyn* 57 686-696 (2022) **DOI:10.1134/S0015462822050123**

[18] Ermolaev, Y.G., Kosinov, A.D., Kocharin, V.L., Semenov, A.N., Semionov, N.V., Shipul', S.A., Yatskikh, A.A. Effect of small angles of attack on laminar-turbulent transition in the supersonic boundary layer on a swept wing with $\chi = 72°$. *Fluid Dyn* 57 30-36 (2022) **DOI:10.1134/S0015462822010037**

[19] Milinovic, M., Jerković, D., Jeremić, O., Kovač, M. Experimental and simulation testing of flight spin stability for small caliber cannon projectile. *Stroj vestn - J Mech E* 58 394-402 (2012) **DOI:10.5545/sv-jme.2011.277**

[20] Lopez-Lopez, A., Robles-Ocampo, J.B., Sevilla-Camacho, P.Y., Lastres-Danguillecourt, O., Muniz, J., Perez-Sarinana, B.Y., de la Cruz, S. Dynamic instability of a wind turbine blade due to large deflections: An experimental validation. *Stroj vestn-J Mech E* 66 523-534 (2020) **DOI:10.5545/sv-jme.2020.6678**

[21] Akbıyık, H., Yavuz, H., Akansu, Y. (2018). A study on the plasma actuator electrode geometry configurations for improvement of the aerodynamic performance of an airfoil. *Stroj vestn-J Mech E* 64, 719-725 **DOI:10.5545/sv-jme.2017.5041**

[22] Balabel, A., Hegab, A.M., Nasr, M., El-Behery, S.M. Assessment of turbulence modeling for gas flow in two-dimensional convergent-divergent rocket nozzle. *Appl Math Model* 35 3408-3422 (2011) **DOI:10.1016/j.apm.2011.01.013**

[23] Luo, T.Y., Yin, J., Lin, X.D., Zu, X.Y., Xiong, B., Bai, B.Q., et al. *Method for obtaining supersonic jet static operation pressure matching point of jet wind tunnel*. China National Knowledge Infrastructure (CNKI) Patent No. 114184349B (2022)

Acknowledgements *The authors wish to acknowledge the financial support of Laboratory of Science and technology on integrated Logistics Support, National University of Defense Technology (WDZC20245150310), Natural Science Foundation of Hu'nan (2024JJ6462), Guangxi Scientific Research Basic Ability Enhancement Project (2024KY0355), Natural Science Foundation of Shandong (ZR2021QE059).*

Received 2024-10-24, revised 2025-03-24, accepted 2025-04-01
as Original Scientific Paper.

Data Availability *The data supporting the findings of this study are included in the article.*

Author Contribution *Peng Liu: writing - original draft, visualization, validation, methodology, investigation, resources; Jinglun Cai: writing - original draft, methodology, investigation, conceptualization, data curation; Xuejing Shao: validation, methodology, conceptualization; Hui Jin: validation, supervision, conceptualization.*

Raziskava hitre metode za določitev ujemajoče se točke statičnega obratovalnega tlaka nadzvočnega curka v vetrovniku

Povzetek *Pri preskusih v vetrovniku lahko neusklajeni obratovalni tlaki povzročijo, da se v toku curka pojavijo ekspanzijski valovi, kompresijski valovi in valovne interference. Trenutne raziskave usklajevanja tlakov v vetrovniku zahtevajo stalno prilagajanje obratovalnih tlakov na vstopu in izstopu, da se doseže idealno razširjeno stanje nadzvočnega curka, kar predstavlja veliko delovno obremenitev. V tej študiji predstavljamo numerično simulacijo toka v nadzvočnem vetrovniku pri različnih izstopnih tlakih na osnovi Reynoldsove metode povprečenih Navier-Stokesovih enačb (RANS). Predlagana je metoda za hitro določitev točke ujemanja statičnega obratovalnega tlaka nadzvočnega curka, s katero lahko hitro ugotovimo ustrezen obratovalni tlak. Kadar je Machovo število kontrolne točke na osi jedrnega območja curka znotraj 5 % standardnega Machovega števila na izstopu šobe, je curek v preskusni komori vetrovnika v stanju idealne ekspanzije. Izstopni tlak v teh razmerah predstavlja standardni obratovalni tlak. Hkrati smo primerjali strukture toka v pogojih prekomerne ekspanzije, idealne ekspanzije in premajhne ekspanzije. Pokazalo se je, da so ključni fizikalni parametri v jedrnem območju nadzvočnega curka v stanju idealne ekspanzije, pridobljene s to hitro metodo, stabilno porazdeljeni, kar omogoča, da enakomerno območje curka preseže meje rombastega območja in zagotovi enakomeren tok znotraj meja nadzvočnega curka.*

Ključne besede *nadzvočni curek, ujemanje tlaka, ekspanzijski val, kompresijski val*